Electronic Supplementary Material (ESI) for Polymer Chemistry


# Supporting Information

## Influence of Chelating Groups and Comononomers on the Merocyanine-Metal Ion Interaction in Spiropyran Containing Copolymer Thin Films

*Kristen. H. Fries, Gareth R. Sheppard, Jenna Bilbrey, Jason Locklin**

**Synthesis of Spiropyran Methyl Methacrylate (SPMA)**

1-(2-Hydroxyethyl)-3-dimethyl-6-nitrospiro(2H-1-benzopyran-2,2-indole (SP alcohol)[1] was subsequently coupled to methacrylic acid following standard procedures.[2]

**Synthesis of 2-Hydroxy-3-Methoxy-5-Nitrobenzaldehyde**

6.00 g (39.4 mmol) of 2-hydroxy-3-methoxybenzaldehyde were added to 40 mL of glacial acetic acid. The solution was cooled to 15 °C with an ice-water bath. A solution of 2.63 mL (63.16 mmol) of concentrated nitric acid and 6.10 mL (106 mmol) of glacial acetic acid was added dropwise over an hour. An orange precipitate formed. The solution was allowed to warm to room temperature and left to stir overnight. The precipitate was filtered, washed with ethanol, and dried on high vacuum. The yellow solid was used without further purification. Yield: 4.5g (75%) $^1$H NMR (300 MHz, DMSO-$d_6$) δ (ppm): 10.36 (s, 1H); 8.13 (s, 1H); 7.95 (s, 1H); 4.02 (s, 3H).

**Synthesis of Methoxy-Substituted Spiropyran Methacrylate (MEO)**

2-(8-methoxy-3',3'-dimethyl-6-nitrospiro[chromene-2,2'-indolin]-1'-yl)ethanol (MEO-OH) was subsequently coupled to methacrylic acid. 4.00 g (10.5 mmol) of MEO-OH and 4.95 g (18.8 mmol) of triphenylphosphine were added to 70 mL of dry THF. The solution was cooled to 0 °C. 1.60 mL (18.8 mmol) of methacrylic acid was added and the solution was stirred for 20 min. While the reaction mixture was still at 0 °C, a solution of 3.03 mL (18.8 mmol) diethyl azodicarboxylate and 10 mL of dry THF was added dropwise over one hour. The reaction mixture was stirred at room temperature for 24 h. The solution was concentrated to dryness using a rotary evaporator. A blue solid was isolated by column chromatography on a neutral alumina column using hexane:ethyl acetate (4:1 v/v) as the eluent. Yield: 3.5 g (87.5%) $^1$H NMR (300 MHz, $CDCl_3$) δ (ppm): 7.68 (s, 1H); 7.61 (s, 1H); 7.18 (t, 1H); 7.06 (d, 1H); 6.87-

6.70 (m, 3H); 6.05 (s, 1H); 5.82 (s, 1H); 5.54 (d, 1H); 4.29 (m, 2H); 3.75 (s, 3H); 3.57 (m, 1H); 3.48 (1H); 1.90 (3H); 1.27 (s, 3H); 1.15 (s, 3H).

**Synthesis of Poly($MMA_{90}$-*co*-$MEO_{10}$)**

MEO (0.408 g, 0.906 mmol), MMA (0.816 g, 8.15 mmol), CuBr (0.005 g, 0.035 mmol), and Et2BriB (0.007 g, 0.035 mmol) were added to a dry, 25 mL schlenk flask. Anhydrous THF (5 mL) was then added, and the solution was degassed under Ar for 2 h. After degassing, PMDETA (0.060 g, 0.346 mmol), which was also degassed under Ar for 2 h, was added to the reaction mixture. The rubber septum on the schlenk flask was then replaced with a glass stopper while still under Ar to avoid any possible oxygen poisoning. The reaction was then placed in an oil bath for 16 h at 65 ºC. The flask was then opened and exposed to air. The solution was precipitated in approximately 50 mL of cold methanol, and the precipitate was filtered through a medium frit funnel. The polymer was re-dissolved in THF and the precipitation repeated. A blue powder was collected ($M_w$ = 29,997 kDa, $M_n$ = 29,103 kDa, $M_w/M_n$ = 1.031, as obtained by gel permeation chromatography). $^1$H NMR (500 MHz, $CDCl_3$) δ (ppm): 8.14 (s, 0.3H); 7.70 (s, 1.4H); 7.62 (s, 1.1H); 7.18 (s, 1.2H); 7.07 (s, 1.2H); 6.89 (s, 2.5H); 6.67 (d, 0.8H); 5.84 (s, 1.00H); 4.06 (s, 3.6H); 3.90 (s, 1.2H); 3.75 (s, 5.5H); 3.59 (s, 17.7H); 3.51 (s, 9H); 1.79 (m, 17.4H); 1.59 (s, 3.8H); 1.40 (s, 1.8H); 1.27 (s, 5.1H); 1.17 (s, 5.2H); 1.01 (s, 9.2H); 0.81 (s, 17.1H).

**Synthesis of Poly($MMA_{70}$-*co*-$MEO_{30}$)**

MEO (0.817 g, 1.81 mmol), MMA (0.452 g, 4.52 mmol), CuBr (0.005 g, 0.035 mmol), and Et2BriB (0.007 g, 0.035 mmol) were added to a dry, 25 mL schlenk flask. Anhydrous THF (5 mL) was then added, and the solution was degassed under Ar for 2 h. After degassing, PMDETA (0.060 g, 0.346 mmol), which was also degassed under Ar for 2 h, was added to the

reaction mixture. The rubber septum on the schlenk flask was then replaced with a glass stopper while still under Ar to avoid any possible oxygen poisoning. The reaction was then placed in an oil bath for 16 h at 65 ºC. The flask was then opened and exposed to air. The solution was precipitated in approximately 50 mL of cold methanol, and the precipitate was filtered through a medium frit funnel. The polymer was re-dissolved in THF and the precipitation repeated. A blue powder was collected ($M_w$ = 35,498 kDa, $M_n$ = 33,467 kDa, $M_w/M_n$ = 1.061, as obtained by gel permeation chromatography). $^1$H NMR (500 MHz, $CDCl_3$) δ (ppm): 8.12 (s, 0.3H); 7.61 – 7.17 (d, 2.4H); 7.08-7.17 (d, 2.8H); 6.87 (s, 2.8H); 6.66 (d, 1H); 6.47 (s, 0.2H); 5.85 (s, 1H); 4.05 (s, 2H); 3.88 (s, 0.9H); 3.72 (s, 3.2H); 3.59 (s, 6.3H); 3.51 (s, 8.3H); 1.78 (m, 7.4H); 1.57 (s, 1.3H); 1.40 (s, 1.2H); 1.27 (m, 4.3H); 1.17 (s, 5.8H); 0.98 (s, 4.8H); 0.81 (s, 8.7H).

**Synthesis of Poly(TFEMA$_{90}$-*co*-MEO$_{10}$)**

MEO (0.408 g, 0.906 mmol), TFEMA (1.37 g, 8.15 mmol), CuBr (0.005 g, 0.035 mmol), and Et2BriB (0.007 g, 0.035 mmol) were added to a dry, 25 mL schlenk flask. Anhydrous THF (5 mL) was then added, and the solution was degassed under Ar for 2 h. After degassing, PMDETA (0.060 g, 0.346 mmol), which was also degassed under Ar for 2 h, was added to the reaction mixture. The rubber septum on the schlenk flask was then replaced with a glass stopper while still under Ar to avoid any possible oxygen poisoning. The reaction was then placed in an oil bath for 16 h at 65 ºC. The flask was then opened and exposed to air. The solution was precipitated in approximately 50 mL of cold methanol, and the precipitate was filtered through a medium frit funnel. The polymer was re-dissolved in THF and the precipitation repeated. A blue powder was collected ($M_w$ = 110,832 kDa, $M_n$ = 95,983 kDa, $M_w/M_n$ = 1.155, as obtained by gel permeation chromatography). $^1$H NMR (500 MHz, $CDCl_3$) δ (ppm): 8.14 (s, 0.4H); 7.73 (d, 1.5H); 7.63 (m, 1.8H); 7.19 (m, 1.8H); 7.08 (m, 2H); 6.95 (s, 0.6H); 6.86 (m, 3.4H); 6.67 (m,

3.4H); 6.47 (s, 0.5H); 5.84 (d, 1H); 4.34 (s, 35H); 4.05 (d, 3.3H); 3.94 (d, 1.5H); 3.75 (m, 7.1H); 3.50 (d, 4.3H); 1.84 – 2.00 (m, 32.5H); 1.61 (s, 7.3H); 1.47 (s, 3.2H); 1.40 (s, 2.6H); 1.27 (m, 7.1H); 1.16 (m, 7H); 1.08 (s, 18H); 0.93 (m, 34H).

**Synthesis of Poly(TFEMA$_{50}$-*co*-MEO$_{50}$)**

MEO (0.785 g, 1.74 mmol), TFEMA (0.29 g, 1.73 mmol), CuBr (0.005 g, 0.035 mmol), and Et2BriB (0.007 g, 0.035 mmol) were added to a dry, 25 mL schlenk flask. Anhydrous THF (5 mL) was then added, and the solution was degassed under Ar for 2 h. After degassing, PMDETA (0.060 g, 0.346 mmol), which was also degassed under Ar for 2 h, was added to the reaction mixture. The rubber septum on the schlenk flask was then replaced with a glass stopper while still under Ar to avoid any possible oxygen poisoning. The reaction was then placed in an oil bath for 16 h at 65 ºC. The flask was then opened and exposed to air. The solution was precipitated in approximately 50 mL of cold methanol, and the precipitate was filtered through a medium frit funnel. The polymer was re-dissolved in THF and the precipitation repeated. A blue powder was collected. $^1$H NMR (500 MHz, $CDCl_3$) δ (ppm): 8.14 (s, 0.6H); 7.61 – 7.67 (d, 3H); 7.08 – 7.13 (d, 3.7H); 6.85 (s, 3.8H); 6.64 (s, 1.1H); 6.50 (s, 0.3H); 5.80 (s, 1H); 4.32 (s, 5.4H); 4.05 (s, 2.8H); 3.84 (s, 1.2H); 3.70 (s, 5H); 3.38 – 3.52 (d, 3.5H); 1.85 (m, 7.9H); 1.38 (s, 2H); 1.26 (s, 5.1H); 1.14 (s, 8.6H); 0.85 (d, 8.2H).

**Synthesis of Poly(TFEMA$_{90}$-*co*-SPMA$_{10}$)**

SPMA (0.381 g, 0.906 mmol), TFEMA (1.37 g, 8.15 mmol), CuBr (0.005 g, 0.035 mmol), and Et2BriB (0.007 g, 0.035 mmol) were added to a dry, 25 mL schlenk flask. Anhydrous THF (5 mL) was then added, and the solution was degassed under Ar for 2 h. After degassing, PMDETA (0.060 g, 0.346 mmol), which was also degassed under Ar for 2 h, was added to the reaction mixture. The rubber septum on the schlenk flask was then replaced with a glass stopper

while still under Ar to avoid any possible oxygen poisoning. The reaction was then placed in an oil bath for 16 h at 65 ºC. The flask was then opened and exposed to air. The solution was precipitated in approximately 50 mL of cold methanol, and the precipitate was filtered through a medium frit funnel. The polymer was re-dissolved in THF and the precipitation repeated. A pink powder was collected. $^1$H NMR (500 MHz, $CDCl_3$) δ (ppm): 8.02 (s, 2H); 7.42 (s, 1H); 7.09 – 7.19 (d, 1H); 6.91 (s, 2H); 6.77 (m, 2H); 5.87 (s, 1H); 4.34 (s, 20H); 4.06 (s, 2H); 3.75 (s, 3.4H); 3.38 – 3.50 (d, 2H); 1.85 – 2.16 (m, 24H); 1.54 (s, 19H); 1.29 (d, 5H); 1.17 (s, 5H); 1.09 (s, 10H); 0.92 (d, 21H).

**Synthesis of Poly(MEO)**

MEO (0.845 g, 3.49 mmol), CuBr (0.005 g, 0.035 mmol), and Et2BriB (0.007 g, 0.035 mmol) were added to a dry, 25 mL schlenk flask. Anhydrous THF was then added, and the solution was degassed under Ar for 2 h. After degassing, PMDETA (0.060 g, 0.346 mmol), which was also degassed under Ar for 2 h, was added to the reaction mixture. The rubber septum on the schlenk flask was then replaced with a glass stopper while still under Ar to avoid any possible oxygen poisoning. The reaction was then placed in a 65 ºC oil bath for 16 h. The flask was then opened and exposed to air. The solution was precipitated in approximately 50 mL of cold methanol. Precipitate was filtered through a medium frit funnel. It was then redissolved in THF and the procedure was repeated. A blue powder was collected (unable to determine molecular weight using gel-permeation chromatography and end group analysis was not possible with $^1$H NMR). $^1$H NMR (500 MHz, $CDCl_3$) δ (ppm): 8.11 (s, 0.2H); 7.54 (s, 2.5H); 6.44 – 7.00 (m, 7H); 5.76 (s, 1H); 4.00 (s, 2.5H); 3.50 (d, 7.7H); 1.62 – 1.85 (m, 2.3H); 1.23 (s, 3.8H); 1.09 (s, 4.6H); 0.75 (s, 3.3H).

**Scheme S1.** Synthetic Route to **MEO** Monomer.

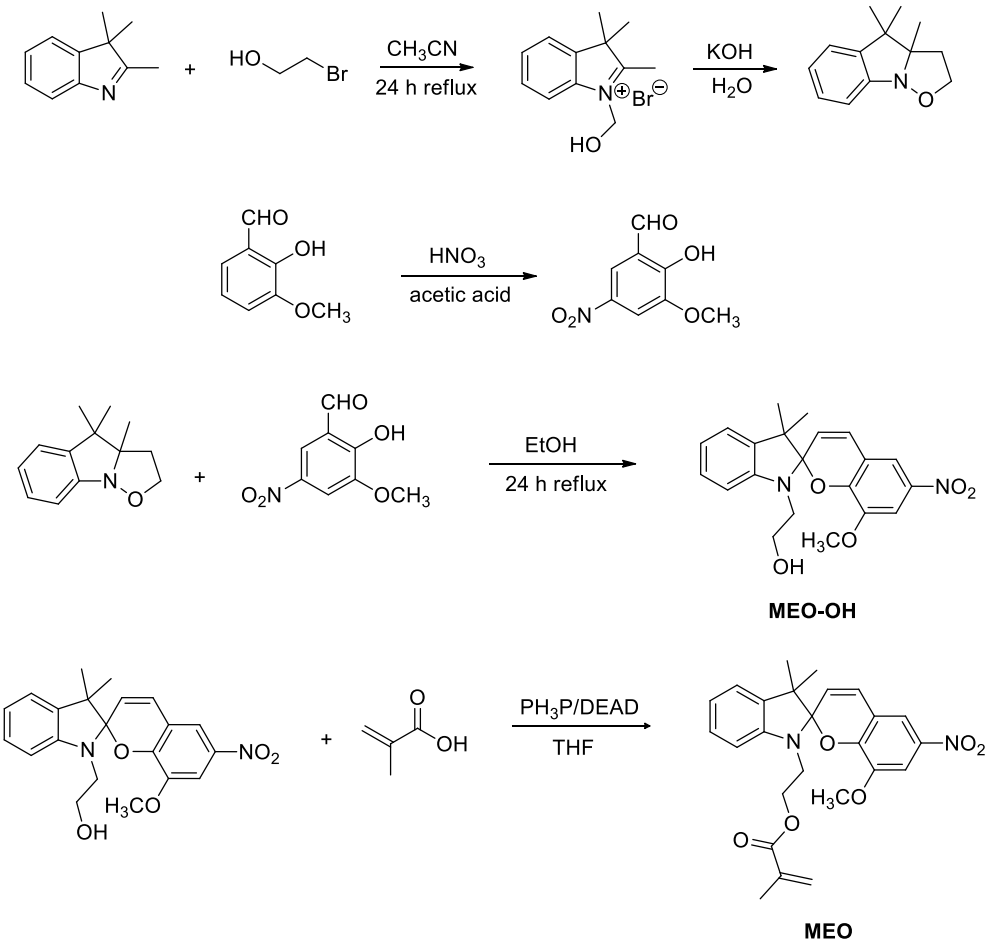

**Table S1.** Main FT-IR frequencies for poly($TFEMA_{90}$-*co*-$MEO_{10}$) before (spiropyran) and after (merocyanine) UV irradiation.

| | Spiropyran | Merocyanine |
|---|---|---|
| **Assignments** | **Wavenumbers ($cm^{-1}$)** | **Wavenumbers ($cm^{-1}$)** |
| C=O | 1748 | 1748 |
| Ar C=C | 1655 | - |
| Ar C=C | 1608 | 1608 |
| $C=N^+$ | - | 1592 |
| $NO_2$ sym stretch | 1525 | 1519 |
| $C-O^-$ | - | 1456 |
| $NO_2$ asym stretch | 1340 | 1340 |
| C-N (tertiary) stretch | 1340 | - |
| $C-N^+$ | - | 1311 |
| $OCH_3$ sym stretch | 1282 | 1283 |
| C-F stretch | 1282 | 1283 |
| C-O-C ether sym stretch | 1282 | - |
| TFEMA | 1230 | 1228 |
| C-O-C ether asym stretch | 1174 | - |
| C-O ester stetch (TFEMA and SPMA) | 1174 | 1173 |
| C-O ester stretch (TFEMA) | 1133 | 1133 |
| $OCH_3$ asym stretch | 1118 | 1118 |
| C-O ester (SPMA) | 1090 | 1090 |
| C-C-N bend | 1070 | - |

**Table S2.** Main FT-IR frequencies for poly(TFEMA$_{90}$-*co*-SPMA$_{10}$) before (spiropyran) and after (merocyanine) UV irradiation.

| | Spiropyran | Merocyanine |
|---|---|---|
| **Assignments** | **Wavenumbers (cm$^{-1}$)** | **Wavenumbers (cm$^{-1}$)** |
| C=O | 1748 | 1748 |
| C=N$^+$ | - | 1592 |
| $NO_2$ sym stretch | 1525 | 1519 |
| C-O$^-$ | - | 1456 |
| $NO_2$ asym stretch | 1340 | 1340 |
| C-N (tertiary) stretch | 1342 | - |
| C-N$^+$ | - | 1311 |
| $OCH_3$ sym | 1282 | 1283 |
| C-F stretch | 1282 | 1283 |
| C-O-C ether sym stretch | 1282 | - |
| TFEMA | 1230 | 1228 |
| C-O-C ether asym stretch | 1174 | - |
| C-O ester stetch (TFEMA and SPMA) | 1174 | 1173 |
| C-O ester stretch (TFEMA) | 1133 | 1133 |
| $OCH_3$ aysm | 1118 | 1118 |
| C-O ester (SPMA) | 1090 | 1090 |
| C-C-N bend | 1070 | - |

**Table S3.** Summary of the $\Delta\lambda_{max}$ for each metal ion when bound to the various copolymer thin films.

| | **Sn$^{2+}$** | **Fe$^{2+}$** | **Cu$^{2+}$** | **Zn$^{2+}$** | **Ni$^{2+}$** | **Co$^{2+}$** |
|---|---|---|---|---|---|---|
| **Poly(MMA$_{90}$-*co*-SPMA$_{10}$)** | 161 nm | 147, 64 nm | 174, 64 nm | 90 nm | 27 nm | 54 nm |
| **Poly(TFEMA$_{90}$-*co*-SPMA$_{10}$)** | 170 nm | 127, 24 nm | 143, 57 nm | 78 nm | 8 nm | 27 nm |
| **Poly(MMA$_{90}$-*co*-MEO$_{10}$)** | 234 nm | 99 nm | 94 nm | 90 nm | 31 nm | 69 nm |
| **Poly(TFEMA$_{90}$-*co*-MEO$_{10}$)** | 124 nm | 25 nm | 83 nm | 72 nm | 11 nm | 37 nm |

**Table S4.** Main FT-IR frequencies for poly(TFEMA$_{90}$-*co*-MEO$_{10}$) when bound to the different metal ions.

| Assignments | $Sn^{2+}$ ($cm^{-1}$) | $Fe^{2+}$ ($cm^{-1}$) | $Cu^{2+}$ ($cm^{-1}$) | $Zn^{2+}$ ($cm^{-1}$) | $Ni^{2+}$ ($cm^{-1}$) | $Co^{2+}$ ($cm^{-1}$) |
|---|---|---|---|---|---|---|
| **C=O** | 1748 | 1748 | 1748 | 1748 | 1748 | 1748 |
| **Ar C=C** | 1645 | 1641 | n/a | 1651 | 1651 | 1651 |
| **Ar C=C** | 1608 | 1609 | n/a | 1606 | 1606 | 1608 |
| **C=N$^+$** | 1592 | 1595 | 1592 | 1592 | 1595 | 1592 |
| **$NO_2$ sym stretch** | 1527 | 1527 | 1526 | 1521 | 1521 | 1521 |
| **$NO_2$ asym stretch** | 1341 | 1341 | 1341 | 1341 | 1341 | 1341 |
| **C-N$^+$** | 1308 | 1311 | 1320 | 1308 | 1318 | 1317 |
| **$OCH_3$ sym stretch** | 1283 | 1283 | 1283 | 1283 | 1283 | 1283 |
| **TFEMA** | 1232 | 1231 | 1231 | 1231 | 1231 | 1231 |
| **C-O ester stretch** | 1174 | 1174 | 1177 | 1174 | 1177 | 1177 |
| **$OCH_3$ asym stretch** | 1118 | 1118 | 1118 | 1118 | 1118 | 1118 |

**Table S5.** Main FT-IR frequencies for poly(TFEMA$_{90}$-*co*-SPMA$_{10}$) when bound to the different metal ions.

| Assignments | $Sn^{2+}$ ($cm^{-1}$) | $Fe^{2+}$ ($cm^{-1}$) | $Cu^{2+}$ ($cm^{-1}$) | $Zn^{2+}$ ($cm^{-1}$) | $Ni^{2+}$ ($cm^{-1}$) | $Co^{2+}$ ($cm^{-1}$) |
|---|---|---|---|---|---|---|
| C=O | 1746 | 1746 | 1746 | 1746 | 1746 | 1746 |
| $C=N^+$ | 1577 | 1593 | 1584 | 1593 | 1593 | 1593 |
| $NO_2$ sym stretch | 1523 | 1518 | 1521 | 1521 | 1518 | 1518 |
| $C-O^-$ | 1450s | 1450s | 1450s | 1450s | 1450s | 1450s |
| $NO_2$ asym stretch | 1343 | 1343 | 1343 | 1343 | 1343 | 1343 |
| $C-N^+$ | 1311 | 1311 | 1311 | 1311 | 1313 | 1313 |
| TFEMA | 1232 | 1231 | 1231 | 1231 | 1231 | 1231 |
| C-O ester stretch (SPMA) | 1090 | 1090 | 1090 | 1090 | 1090 | 1090 |

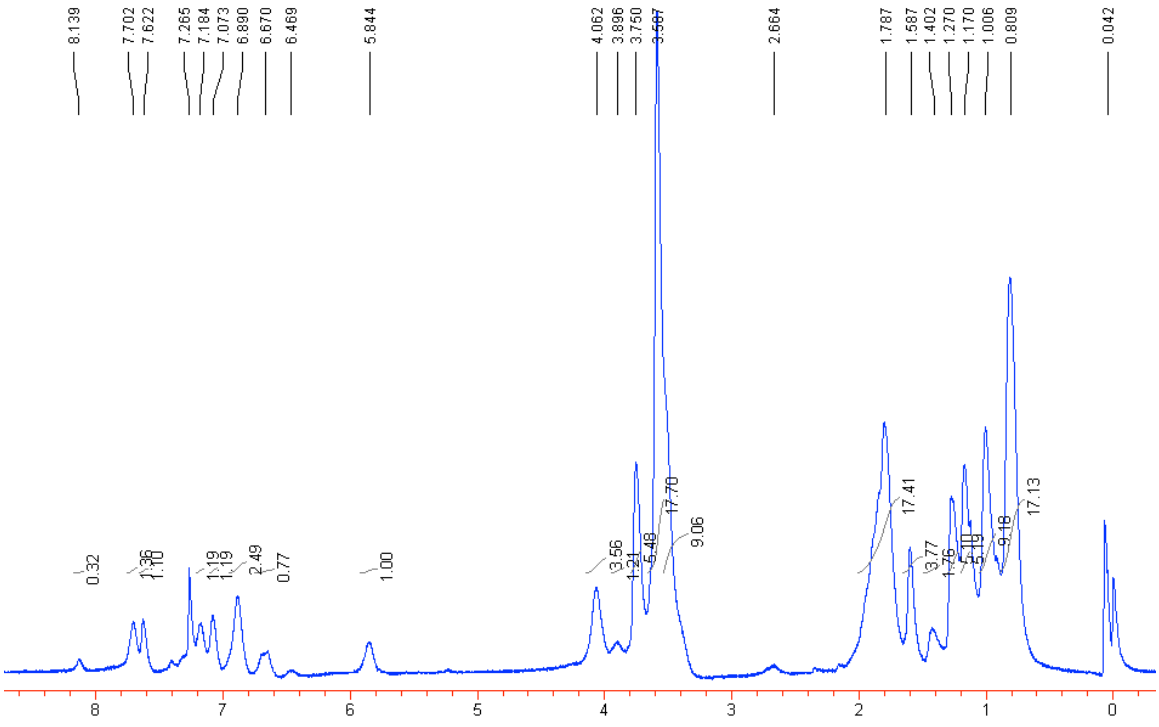


**Figure S1**. NMR spectra of 10 mol% MEO – 90 mol% MMA.

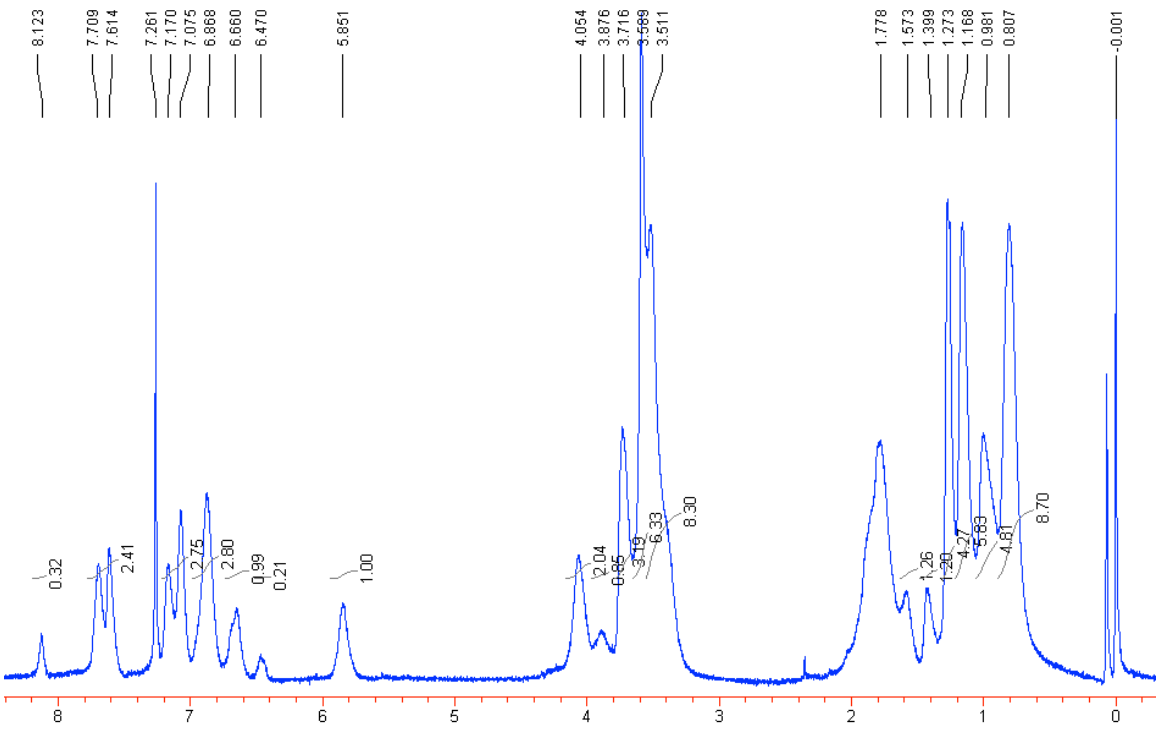


**Figure S2.** NMR spectra of 30 mol% MEO – 70 mol% MMA.

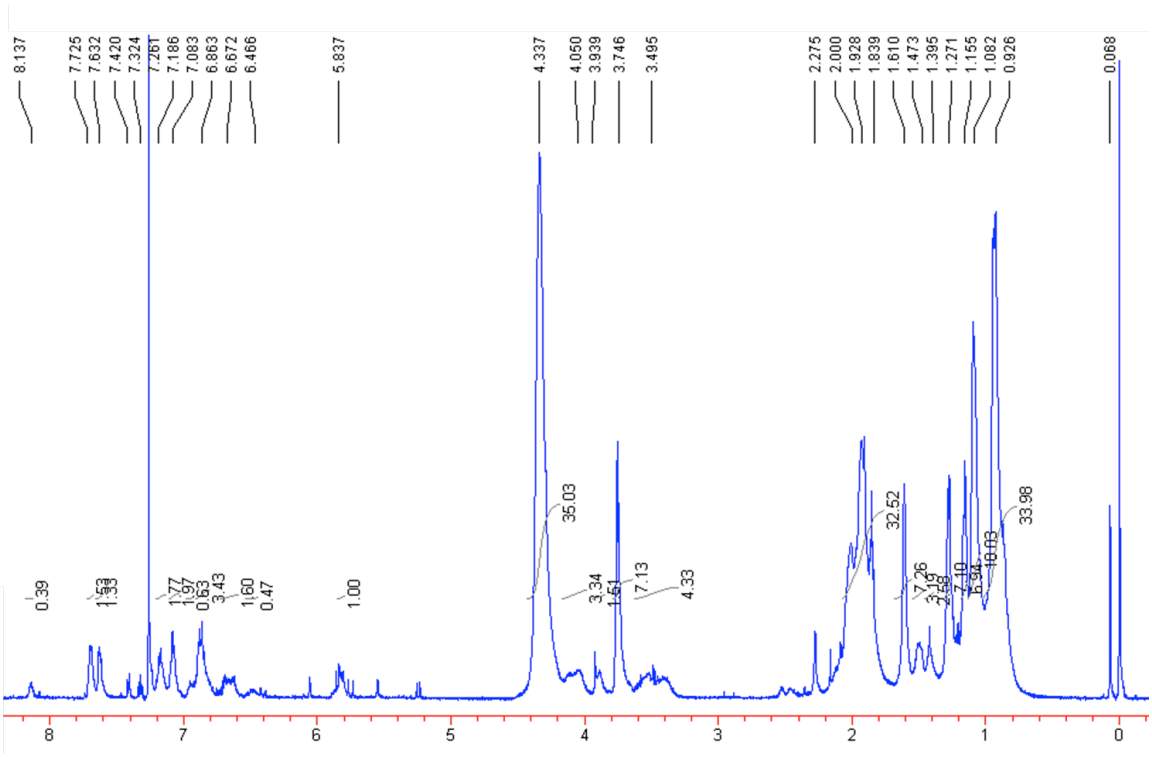


**Figure S3.** NMR spectra of 10 mol% MEO – 90 mol% TFEMA.

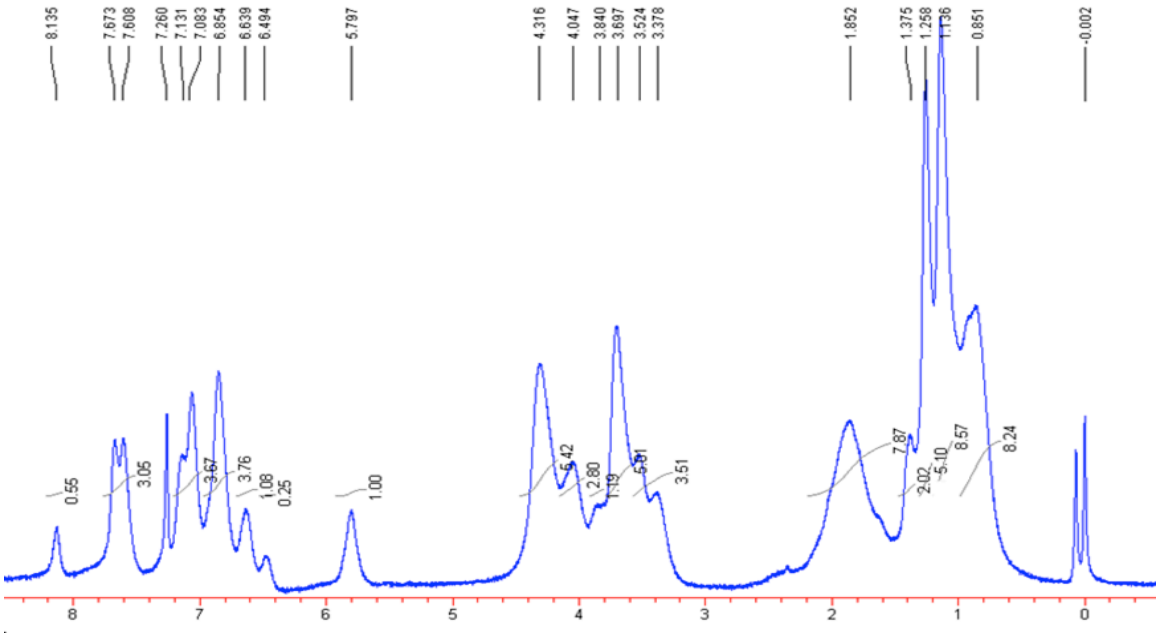


**Figure S4**. NMR spectra of 50 mol% MEO – 50 mol% TFEMA.

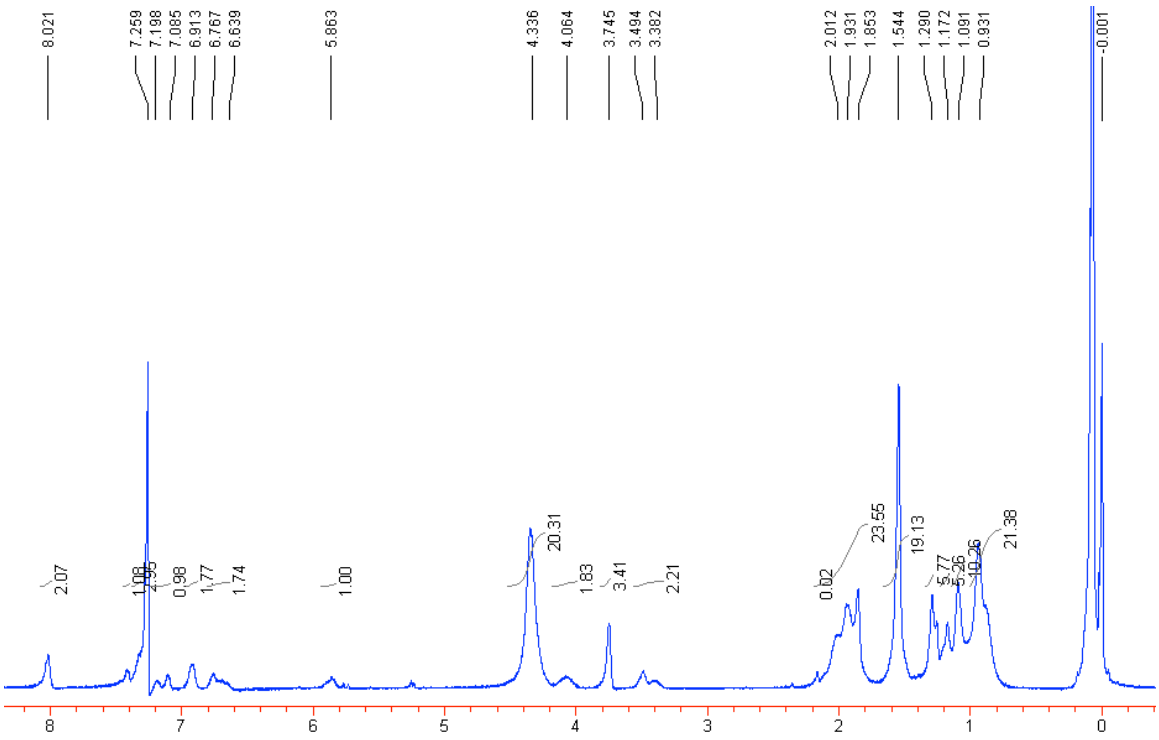


**Figure S5**. NMR spectra of 10 mol% SPMA – 90 mol% TFEMA.

**Chemometric Data Analysis**

FT-IR and UV-visible absorption spectra were analyzed using chemometric methods to aid in spectral interpretation with respect to molecular conformation. MATLAB 7.5 environment (The Mathworks, Inc., Natick, MA) was utilized for spectral pretreatment and principal component analysis (PCA).

**Spectral Preprocessing**

Several spectroscopic pretreatments were investigated to optimize qualitative and quantitative predictive models. Spectral range, baseline correction, normalization, mean centering, and combinations of these steps were explored to optimize the PCA models. Using a leave-one-out cross validation algorithm, minimization of the root mean square error of cross validation (RMSECV) was used as the criterion to identify the optimum preprocessing steps. Optimal preprocessing of the IR dataset consisted of analyzing the spectral range of 1000-1800 $cm^{-1}$ by taking the $2^{nd}$ derivative of each spectrum using a fifteen-point, $2^{nd}$-order polynomial Savitzky-Golay algorithm, followed by normalization to unit-vector length and mean centering.

**Principal Component Analysis**

PCA was used as an unsupervised method to explore variation in the sample spectra and to visualize clustering of similar spectra.[3] PCA models were built using the IR data for pre- and post-UV irradiated polymer films and FT-IR spectra for the polymer films complexed to each of the six metal ions, as well as the nonbinding polymer film. PC scores plots were constructed to search for clustering of samples according to their identity. Loadings plots for the FT-IR datasets identified the spectral bands responsible for spectral variation to aid interpretation of conformational changes due to metal ion complexation and determine differences in binding among the metal ions

**TFEMA90-coMEO10**

Principal component analysis was used to analyze the FT-IR spectra for multiple spin-coated films of poly($TFEMA_{90}$-*co*-$MEO_{10}$) before and after UV irradiation. PCA involves finding combinations of latent variables, or factors, which describe the key trends in the data. It computes a new orthogonal coordinate system from the latent variables, such that new principal components (PC) axes, which are linear combinations of the original, *n*, axis, describe the maximum variance in the data set. PCA allows visualization of clusters of similar spectra to assess spectral reproducibility, identification of different sample types, and identification of variables responsible for spectral differences that can be interpreted with respect to chemical or physical phenomenon. For each data set, FT-IR spectra were obtained before and after UV irradiation for five poly($TFEMA_{90}$-*co*-$MEO_{10}$) spin-coated films. The spectra were preprocessed using standard methods described above (experimental section) prior to performing PCA. A single principal component, PC1, describes 95.2 % of the spectral variance in the data set. A plot of the scores on PC1 shows an obvious separation in the spectra acquired before and after UV irradiation (Fig. 2). In addition, spectra collected for the same sample type cluster tightly, indicating the reproducibility in the preparation method of the thin films, as well as, the consistency of the photoinduced conversion from SP to MC.

Evaluation of the loadings on PC1 provides information regarding the contribution of each wavenumber in the FT-IR spectra to the newly defined PC1 axis. Effectively, these are the wavenumbers responsible for the observed separation along PC1. The PC1 loadings plot (Fig. S6, ESI†) identifies the bands corresponding to the $C\text{-}N^+$, tertiary C-N, and symmetric $NO_2$ stretches (1311, 1340, and 1525 $cm^{-1}$, respectively) as the most significant variation between pre and post UV irradiation.

Other noteworthy bands are the symmetric and asymmetric alkyl aryl ether (-$OCH_3$) stretches at 1282 and 1118 $cm^{-1}$, respectively. The band assigned to the asymmetric C-O-C ether stretch at 1174 $cm^{-1}$ can also be identified. The symmetric C-O-C ether stretch is masked by the strong C-F stretch of the TFEMA copolymer (1282 $cm^{-1}$), so no change in this band is observed upon UV irradiation. It is important to note the phenolate anion stretch is also masked by a band from TFEMA, and as such, the appearance of the phenolic oxygen cannot be seen in the FT-IR spectra. These results are consistent with the ring-opening of SP to MC and the results provided in Table S1 in the ESI†.

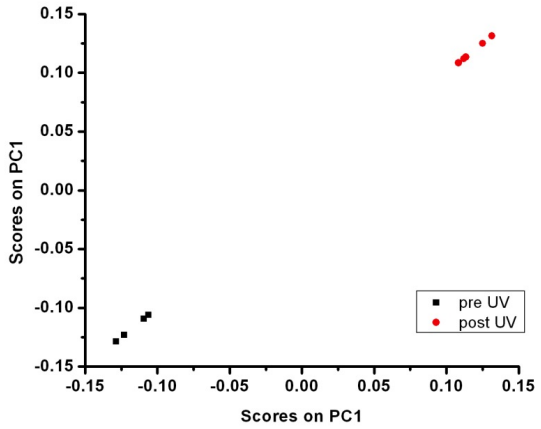


**Fig. 2** Scores plot for PC1 computed from the FT-IR spectra of poly($TFEMA_{90}$-*co*-$MEO_{10}$) before UV irradiation (black) and after UV irradiation (red) for independently prepared films.

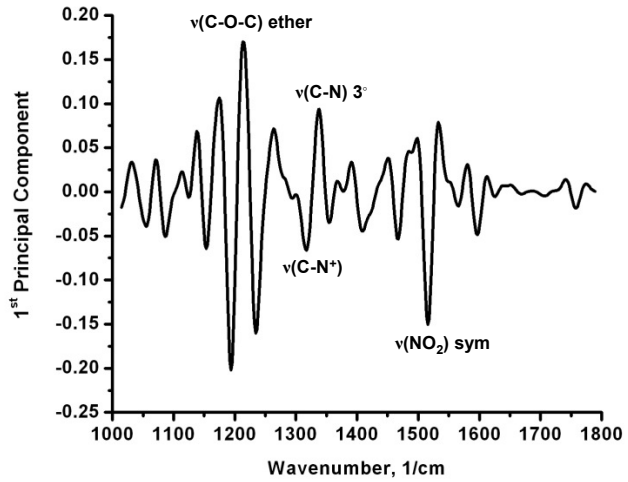


Figure S6. Loadings plot for PC1 computed from spectra of pre- and post-UV irradiated poly(TFEMA$_{90}$-*co*-MEO$_{10}$).

**TFEMA90-co-SPMA10**

PCA was also used to analyze the FT-IR spectra and identify the bands that are important to the ring-opening process. One principal component, PC1, describes 96.8% of the spectral variance in the data set. Fig. 4 shows a plot of the scores on PC1, where there is a distinct separation between the spectra of the ring-closed spiropyran and the spectra of the ring-opened merocyanine. The loadings on PC1 are plotted in Fig. S7 and show that the bands identified as important to the ring-opening process are very similar to those identified for the poly(TFEMA$_{90}$-*co*-MEO$_{10}$) thin film (Fig. S6, ESI†).

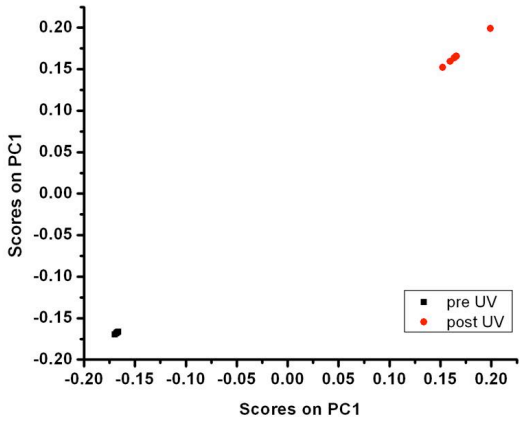


**Fig. 4** Scores plot for PC1 computed from the FT-IR spectra of poly(TFEMA$_{90}$-*co*-SPMA$_{10}$) before UV irradiation (black) and after UV irradiation (red) for independently prepared films.

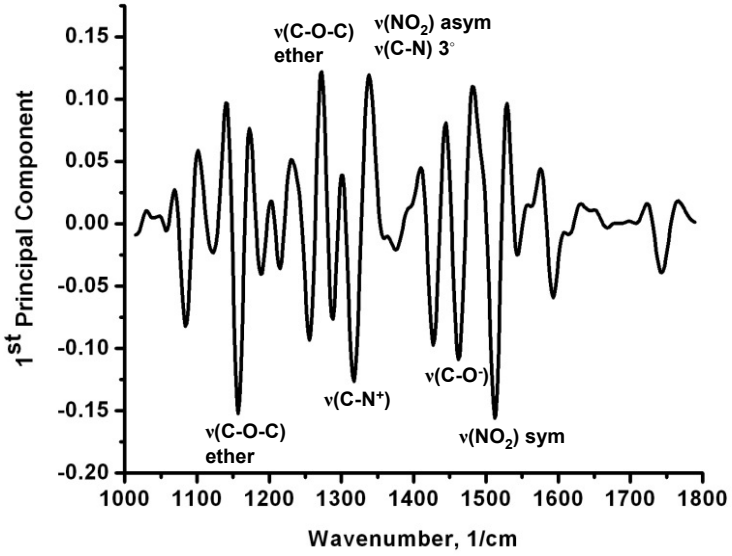


**Figure S7.** Loadings plot for PC1 computed from spectra of pre- and post-UV irradiated poly(TFEMA$_{90}$-*co*-SPMA$_{10}$).

**TFEMA90-co-MEO10 with M2+**

In order to assess the reproducibility of the spectra and elucidate the binding interaction for each metal ion, PCA was performed on the spectra for each merocyanine-metal ion complex. PCA scores plots for PC1 and PC2 are shown in Fig. 11. It can be seen from the plot of the scores on PC2 versus PC1 that spectra for each of the metal ion complexes cluster tightly, signifying the reproducibility of the spectral collection. Moreover, most of the clusters on PC1 are easily resolved from each other. The scores on PC1 reveal that while the FT-IR spectra for the MC-$Co^{2+}$ and MC-$Ni^{2+}$ complexes are very similar, the other complexes can be distinguished from each other, as well as the nonbinding merocyanine. Interestingly, with the exception of $Fe^{2+}$, the scores on PC1 correlate with the hypsochromic shifts seen in the UV-vis spectra (Fig. 8) of the poly($TFEMA_{90}$-*co*-$MEO_{10}$) bound to each metal ion. The MC-$Sn^{2+}$ and MC-$Cu^{2+}$ complexes give the largest blue shift in absorbance maxima, while the absorbance maxima for the MC-$Co^{2+}$ and MC-$Ni^{2+}$ complexes remain very close to the absorbance for the nonbinding merocyanine. Scores on PC2 do not show any more separation between the complexes than on PC1, and as such are not used to describe the data further.

The peaks that contribute to the differences between the clusters, as identified by the loadings on PC1 (Fig. S8, ESI†), are assigned to the symmetrical and asymmetrical stretching of the methoxy group (1118 and 1283 $cm^{-1}$), the C-O ester stretch (1174 $cm^{-1}$), the symmetrical stretch of the aryl nitro group (1520 $cm^{-1}$), the aromatic C=C stretch (1608 $cm^{-1}$), and the $C=N^{+}$ stretching band (1592 $cm^{-1}$). In analyzing the loadings plot for PC1, it is clear the peaks assigned to the aryl methoxy bands are not as important as some of the others. It is significant to note, however, that the C-F stretch (1283 $cm^{-1}$) and the ester C-O stretch (1174 $cm^{-1}$) from the TFEMA

copolymer overshadow the symmetric and asymmetric methoxy stretch at 1283 $cm^{-1}$ and 1174 $cm^{-1}$, respectively, which makes it more difficult to observe the changes in the band shape and frequency upon binding to the metal ions. It is also nearly impossible to observe changes in the band assigned to the phenolate anion as it is masked by a peak associated with the TFEMA in the copolymer.

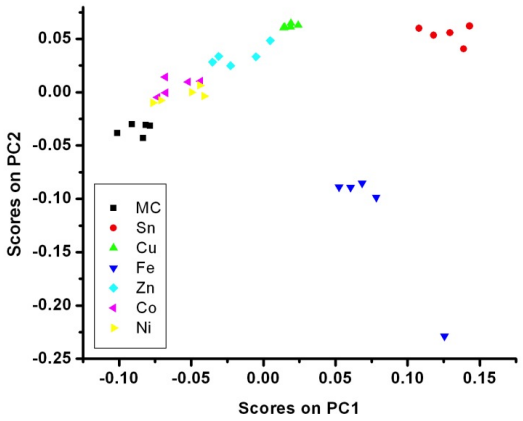


**Fig. 11** Scores plot for PC2 versus PC1 for the PCA model computed from the FT-IR spectra of poly($TFEMA_{90}$-*co*-$MEO_{10}$) after UV irradiation, after binding to $Sn^{2+}$, after binding to $Cu^{2+}$, after binding to $Fe^{2+}$, after binding to $Zn^{2+}$, after binding to $Co^{2+}$, and after binding to $Ni^{2+}$.

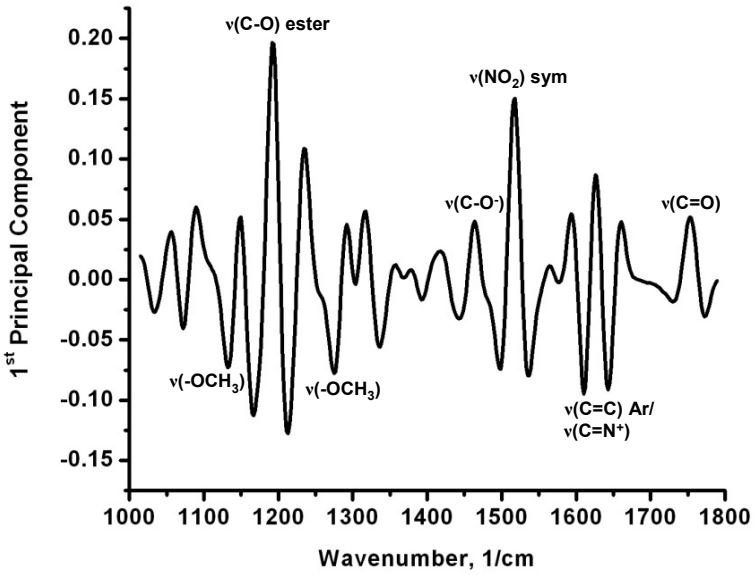


**Figure S8.** Loadings plot for PC1 computed from the PCA model built using FT-IR spectra of poly(TFEMA$_{90}$-*co*-MEO$_{10}$) after UV irradiation, after binding to $Sn^{2+}$, after binding to $Fe^{2+}$, after binding to $Cu^{2+}$, after binding to $Zn^{2+}$, after binding to $Ni^{2+}$, and after binding to $Co^{2+}$.

**TFEMA90-co-SPMA10 with M2+**

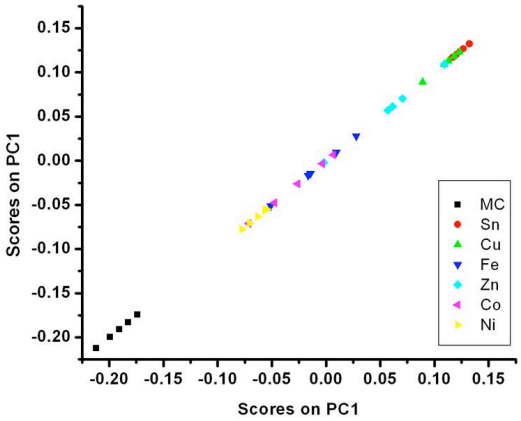

Fig. 13 Scores plot for PC1 versus PC1 for the PCA model computed from the FT-IR spectra of poly(TFEMA$_{90}$-*co*-SPMA$_{10}$) after UV irradiation, after binding to $Sn^{2+}$, after binding to $Cu^{2+}$, after binding to $Fe^{2+}$, after binding to $Zn^{2+}$, after binding to $Co^{2+}$, and after binding to $Ni^{2+}$.

PCA was used to analyze the FT-IR spectra for the poly(TFEMA$_{90}$-*co*-SPMA$_{10}$) thin film when bound to the metal ions to better understand the binding interaction between MC and each ion. Fig. 13 shows the plot of scores on PC1 versus PC1. In this case, the spectra do not cluster as tightly as with poly(TFEMA$_{90}$-*co*-MEO$_{10}$) films when bound to metal ions, but distinctions between several of the complexes are still observed. The plot shows that the MC-$Ni^{2+}$ and the MC-$Co^{2+}$ complexes are very similar, as well as the MC-$Cu^{2+}$ and the MC-$Sn^{2+}$ complexes. It is still possible, however, to see a separation between each of these pairs as well as the rest of the MC-$M^{2+}$ complexes and the nonbinding merocyanine. Again, interestingly, with the exception of the MC-$Fe^{2+}$, the scores on PC1 directly correlate with the UV-vis spectra (Fig. 7) of the MC-$M^{2+}$ complexes. The MC-$Sn^{2+}$ and the MC-$Cu^{2+}$ complexes yield the largest blue shift in absorbance maxima from the nonbinding merocyanine, while the MC-$Co^{2+}$ and MC-$Ni^{2+}$ complex are similar to merocyanine. The peaks that contribute to the differences between the clusters, as identified by the loadings on PC1 (Fig. S9, ESI†), are assigned to the ester C-O stretch in SPMA (1090 $cm^{-1}$), the ester C-O stretch for both TFEMA and SPMA (1176 $cm^{-1}$), the C-$N^+$ band (1311 $cm^{-1}$), the symmetrical and asymmetrical aryl nitro stretching band (1523 and 1342 $cm^{-1}$, respectively), the phenolate anion (1450 $cm^{-1}$), and the carbonyl of the ester side chain (1746 $cm^{-1}$). The aromatic C=C stretching of poly(TFEMA$_{90}$-*co*-SPMA$_{10}$) is not affected by the metal ion binding, as it is for poly(TFEMA$_{90}$-*co*-MEO$_{10}$) when bound to metal ions. These results provide further proof that with the introduction of a second chelating group on the

nitro ring, the carbonyl of the ester side chain is no longer involved in the binding between MC and the metal ions, with the exception of $Sn^{2+}$.

PCA shows that the bands assigned to the aromatic C=C stretching are responsible for a significant amount of variation in the FT-IR spectra of the different MC-$M^{2+}$ complexes for poly(TFEMA$_{90}$-*co*-MEO$_{10}$).

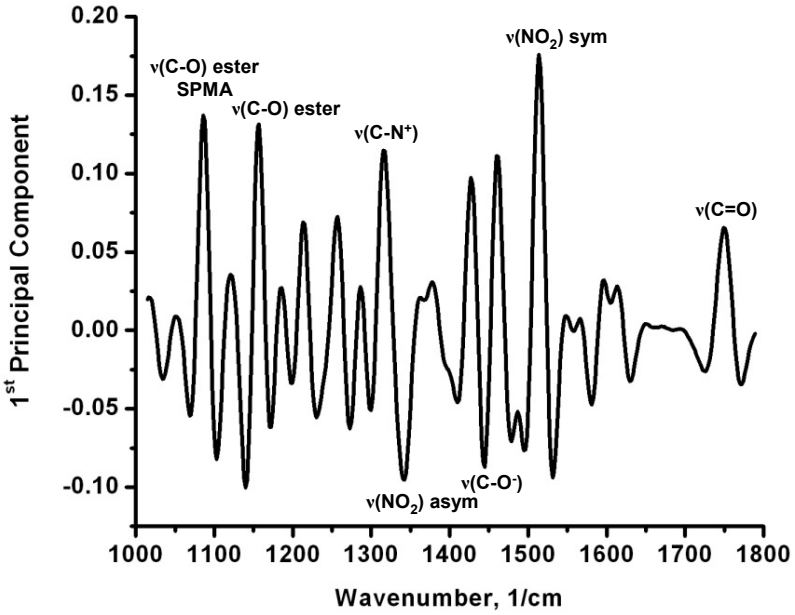


**Figure S9.** Loadings plot for PC1 computed from the PCA model built using FT-IR spectra of poly(TFEMA$_{90}$-*co*-SPMA$_{10}$) after UV irradiation, after binding to $Sn^{2+}$, after binding to $Fe^{2+}$, after binding to $Cu^{2+}$, after binding to $Zn^{2+}$, after binding to $Ni^{2+}$, and after binding to $Co^{2+}$.

**REFERENCES**

(1) Hirshberg, Y. *J. Am. Chem. Soc.* **1956**, *78*, 2304.
(2) Chung, D.-J.; Ito, Y.; Imanishi, Y. *J. Appl. Polym. Sci.* **1994**, *51*, 2027.
(3) Beebe, K. R.; Pell, R. J.; Seasholtz, M. B. *Chemometrics: A Practical Guide*; John Wiley & Sons: New York, 1998.